Swansea University
Prifysgol Abertawe

Cronfa
Setting Research Free

Cronfa - Swansea University Open Access Repository

This is an author produced version of a paper published in :
IEEE Transactions on Energy Conversion

Cronfa URL for this paper:
http://cronfa.swan.ac.uk/Record/cronfa32722

Paper:
Fazeli, M. & Holland, P. (2017). Universal and Seamless Control of Distributed Resources-Energy Storage for all Operational Scenarios of Microgrids. *IEEE Transactions on Energy Conversion*, 1-1.
http://dx.doi.org/10.1109/TEC.2017.2689505

This article is brought to you by Swansea University. Any person downloading material is agreeing to abide by the terms of the repository licence. Authors are personally responsible for adhering to publisher restrictions or conditions. When uploading content they are required to comply with their publisher agreement and the SHERPA RoMEO database to judge whether or not it is copyright safe to add this version of the paper to this repository.
http://www.swansea.ac.uk/iss/researchsupport/cronfa-support/

Universal and Seamless Control of Distributed Resources-Energy Storage for all Operational Scenarios of Microgrids

Megdad Fazeli, *Member, IEEE*, Petar Igic, Senior *Member, IEEE* and Paul Holland *Member, IEEE*

***Abstract*— This paper proposes one control paradigm that can operate in both grid-connected and islanded modes, hence, does not need any sort of islanding detection method. The proposed method automatically and seamlessly rides-through a fault on the grid side, and controls the microgrid's voltage and frequency during islanded operation. During islanded operation it utilises the combination of distributed generation-energy storage similar to the prime-mover of a synchronous generator to control the frequency. A comprehensive active and reactive power control is proposed that minimises the usage of a local fossil-fuelled auxiliary generator. The method is based on expanding the so called non-detection zone to all operational scenarios including islanded mode, hence, having small, "undetectable" voltage and frequency deviation. As soon as the grid is reconnected the distributed generator is automatically and seamlessly synchronised with the grid. This is achieved through keeping PLL as part of the operation in islanded mode without altering its phase angle. The proposed method is validated using PSCAD/ EMTDC simulation.**

***Index Terms*— Islanding detection, Non detection zone, Droop control, Distributed Generation, Microgrids**

I. Introduction

MICROGRID is an integrated energy delivery system that consists of interconnected distributed generation (DG) and storage units which can operate in parallel with or isolated from the main power grid [1]-[3]. Microgrids can benefit customers through providing uninterruptible power, enhancing local reliability, reducing transmission loss, and supporting local voltage and frequency [2]-[6]. To realize these advantages, microgrids must be designed such that they can operate in both grid-connected and islanded (i.e. disconnected from the grid) modes. Therefore, four operating scenarios can be defined for a microgrid: grid-connected, islanded, transition from grid-connected to islanded, and transition from islanded to grid connected [1], [4], [7,] [8]. In grid-connected mode, where voltage and frequency are imposed by the main grid, the imbalance between generated and demanded local active and reactive power will be supplied/absorbed by the grid. In islanded mode, the active and reactive power imbalance must be handled locally. This is usually achieved through using energy storage (ES) systems and auxiliary generators (AG) [2], [3], [9] for active power imbalance, and exploiting the power electronic converters (PEC) of DGs [10] and AGs, to supply/absorb reactive power imbalance. This means that the microgrid's voltage and frequency must be locally controlled within limits defined by international standards such as IEEE 1547 [11]. Transition from islanded to grid-connected is usually handled through utilisation of a Phase Locked Loop (PLL) in order to synchronise DG units to the grid frequency [12]-[14]. Grid reconnection is always intentional. However, grid disconnection (islanded) can be either planned (e.g. for maintenance) or unplanned (e.g. due to a fault on the grid side). According to the present regulations all distributed generation and storage units must be disconnected from the grid within a specified time interval after an islanding event being detected (e.g. within 2 seconds according to IEEE 1547 [1], [7], [11]). However, this undermines the whole concept of the microgrid, which must be able to supply local loads (or at least the critical loads) even after being disconnected from the grid [1], [7]. Therefore, a microgrid must be able to detect an unplanned islanding event in order to switch from grid-connect mode to islanded mode. Islanding detection methods can be categorized into three groups: passive, active, and communication-based. In passive methods, one or more local parameters are monitored in order to detect an islanding event. Different parameters have been proposed in the literature, for example, voltage and frequency [15], unusual changes of active power and frequency [16], fast increases in the voltage phase [17], reactive power [18], difference in phase angle [19] or THD [20]. However, passive methods suffer from a relatively large non detection zone (NDZ). NDZ refers to a certain area in active power vs reactive power plane which is associated to very small, "undetectable" deviation of voltage and frequency [1], [7]. In active methods a controlled disturbance is injected into the system and islanding being detected according to the response of the system [21]-[25]. Although active methods have zero (or very small) NDZ, they tend to be slower than passive methods (due to the dynamics of the system) [7]. In addition, active methods can deteriorate the power quality with the injected disturbance [1], [7].

Manuscript received July 27, 2016; revised…..; accepted….. . This work was supported by the WEFO-ERDF funded project of FLEXIS.

Meghdad Fazeli is a Lecturer at Swansea University, Swansea, UK, (e-mail: m.fazeli@swansea.ac.uk).

Petar Igic is an Associate Professor at Swansea University, Swansea UK, (e-mail: p.igic@swansea.ac.uk).

Paul Holland is an Associate Professor at Swansea University, Swansea, UK, (e-mail: p.m.holland@swansea.ac.uk).

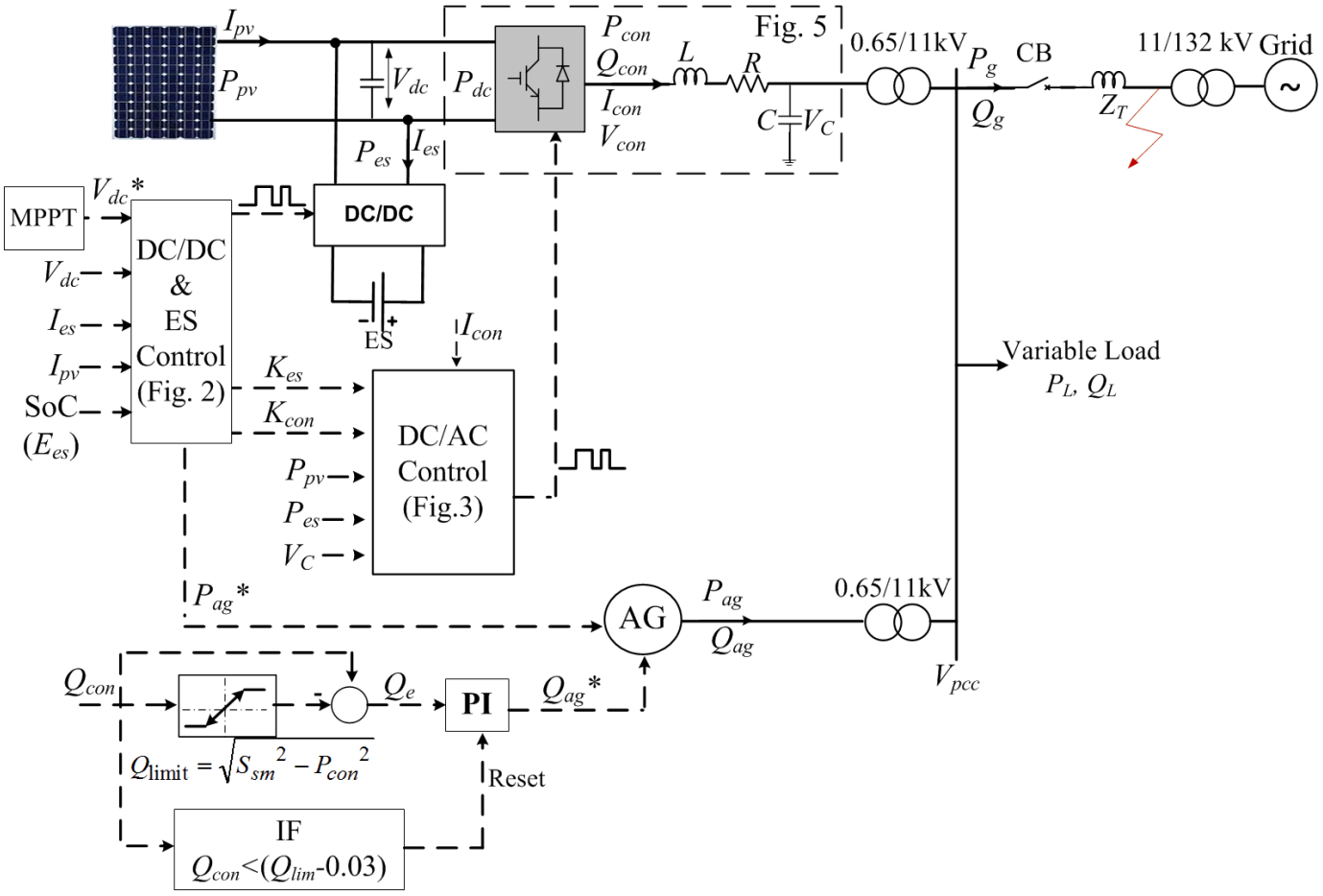

Fig. 1. Proposed control scheme for both grid-connected and islanded modes

The main disadvantage of communication-based methods is that they fully depend on fast and reliable communications between the main grid and DGs, which can be very expensive. Furthermore, any communication method can be subject to noise and disruptions that can endanger the operation.

NDZ refers to the situation that active and reactive powers' imbalance is so small that voltage and frequency does not "detectably" change. The question is why it is a problem? NDZ becomes a problem because there are two control structures (i.e. grid-connected and islanded), hence, microgrids must be able to quickly detect an islanding event in order to switch from grid-connected to islanded mode. This paper proposes one control paradigm for DG-ES-AG systems, which can operate in both grid-connected and islanded modes, and thus, nullifies the problem associate with NDZ. In other words, the proposed method expands the so called NDZ through keeping the active and reactive powers' imbalance such small that voltage and frequency remain within the acceptable limits defined by the standards. The proposed method offers a comprehensive active and reactive power management scheme which minimises the usage of a fossil-fuelled AG, while making sure that the rating of the converter of the DG (S_{rating}) is not violated.

There are less than a handful of previous arts that propose one control paradigm for both grid-connected and islanded operation scenarios, which, to the best of the authors' knowledge, are [26]-[30]. The common idea of all of these papers is to make the DG's inverter operates similar to a synchronous generator. Their common drawback, beside their unnecessary complexity, is that they do not propose a comprehensive active and reactive power management scheme during islanded operation. Moreover, although these arts claim to propose methods applicable for renewable sources, they do not discuss, nor present in their results, issues such as maximum power point tracking (MPPT) and ES control. This is particularly important because their proposed methods usually utilise parameters (such as d-component current in [26]) which are conventionally used for MPPT, without providing any alternative method. The previous arts attempt to control frequency through directly altering the inverter phase angle either through the PLL's angle in [26]-[28], or directly through the PWM reference waveform in [29] and [30]. The missing point is that the rotor angle of a synchronous generator varies indirectly through changing the input mechanical power, not directly through frequency. Similarly, there is no need, in DG, to alter the phase angle directly, which may cause re-synchronisation problems. References [29] and [30] directly control the PWM reference waveform through removing the conventional current control. This can have an adverse effect on over-current protection especially during grid reconnection [30].

The proposed method in this paper (1) offers a comprehensive active and reactive power management scheme, which also includes MPPT and ES control. (2) Keeps PLL part of the control scheme during islanding operation without altering its angle; hence re-synchronisation happens automatically and seamlessly. (3) Uses conventional *d-q* current controlled-VSC, which simplifies implementation and over current protection. (4) Does not require any communication between the grid and the microgrid.

II. Proposed Method

The proposed method will be explained for microgrids with PV systems; however, the control scheme is fully applicable to any other renewable sources including wind and tidal generators. Fig. 1 illustrates the proposed control scheme for a microgrid consisting of DG (PV), energy storage (ES) mechanism (battery), variable loads and an auxiliary generator (AG, e.g. a micro-turbine).

A. DC/DC and ES Control

The ES is connected to the DC link of the PV system through a DC/DC converter. The ES is simulated by a battery; however, the proposed method can be applied on other ES mechanisms. The DC/DC converter is controlled to track maximum PV power. The MPPT method used in this paper was developed in [31], however, other MPPT methods are also applicable. Fig. 2.a illustrates the DC/DC converter control, which uses the classical cascaded voltage and current loops, developed in [31], to control the DC-link voltage V_{dc} to follow its reference (V_{dc}^*) which comes from the MPPT algorithm. Fig. 2.b illustrates the proposed energy management system (EMS) according to the level of battery's state of the charge (SoC). It is noted that if other types of ES systems are to be used, their energy level (E_{es}) can be used instead of SoC. As illustrated in Fig. 2.b, the EMS operates through defining four variable gains based on the level of SoC:

The combined cooperation of ES gain (K_{es}) and converter gain (K_{con}, K_{con}=1-K_{es}) determines how much of the generated PV power (P_{pv}) being stored in ES (P_{es}) or being passed through DC/AC converter (P_{con}), as shown in Fig. 3. When SoC is more than a threshold (e.g. 90%), all P_{pv} must go through DC/AC converter and for SoC less than a threshold (e.g. 10%) all P_{pv} will go to the ES. Hence, If:

SoC > 90% → K_{es}=0 and K_{con}=1

SoC<10% → K_{es}=1 and K_{con}=0

10%<Soc<90% → K_{es} and K_{con} vary between the two points, as shown in Fig. 2.b.

Note that these thresholds are just suggestions and they can change according to the preferences of owner/operator of the DG (e.g. how much energy they want to store in ES determines the high threshold), practical limitations of ES mechanisms, and the defined regulations and standards.

In islanded mode if P_L>P_{pv}, SoC keeps reducing. When SoC becomes less than a threshold (which must be more than the low threshold of K_{es} e.g. 30%, in Fig. 2.b), a power demand signal P_{ag}^* will be sent to the AG as shown in Fig. 1 and Fig. 2.b. For SoC less than a lower threshold (e.g. 5%), P_{ag}^*=1 pu; in order to make sure that ES does not get fully discharged.

Finally, in islanded mode if load power P_L<P_{pv}, SoC keeps increasing. Thus, measures must be taken into account to make sure that the ES will not get over-charged. Previous arts proposed to use a "dumping" resistor to dissipate the extra generated energy. This paper proposes to reduce generation rather than dumping it: as SoC increases more than a threshold (which must be higher than K_{es} high threshold e.g. 95%, in Fig. 2.b), a gain (K_d) will be added to V_{dc}^* (Fig. 2). Since, V_{dc}^* is the voltage at which P_{pv} is at maximum point, P_{pv} will be reduced through adding K_d to V_{dc}^*. The rate at which K_d increases depends on the P_{pv}-V_{dc} characteristic of the PV array. The first order filter (Fig. 2.b) is used to add a dynamic to the system and helps to damp the oscillations ($\tau_d = 0.05$ shows acceptable results).

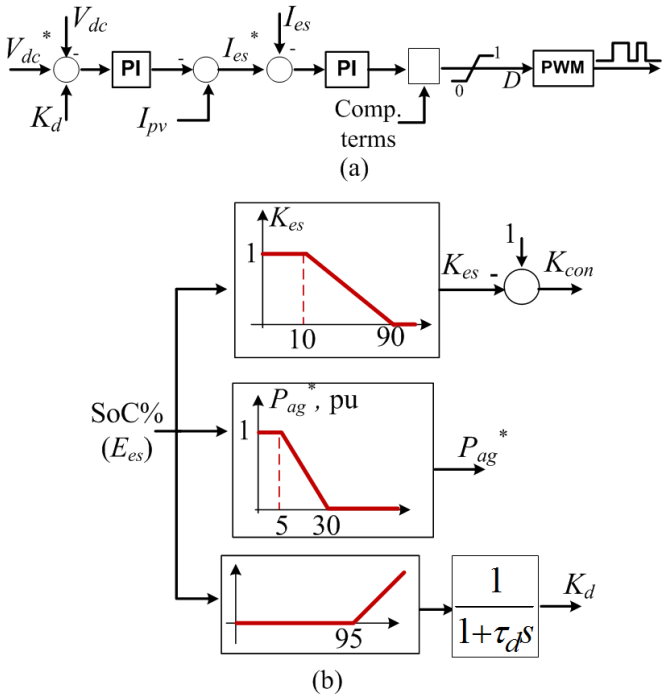

Fig. 2. DC/DC and ES control shown in Fig. 1 (a): DC/DC controller to track MPP of PV, developed in [31] (b) proposed energy management scheme

It is emphasised again that these thresholds are just some suggestions, which may differ from one system to another. For instance, the high threshold of P_{ag}^* (e.g. 30%, in Fig. 2.b), depends on different parameters such as the battery's AHr characteristic and the dynamics of the AG.

B. DC/AC Converter Control

Fig. 3 illustrates the proposed control paradigm for the DC/AC converter shown in Fig. 1. The control, which is based on the standard *d-q* current controllers, is aimed to:

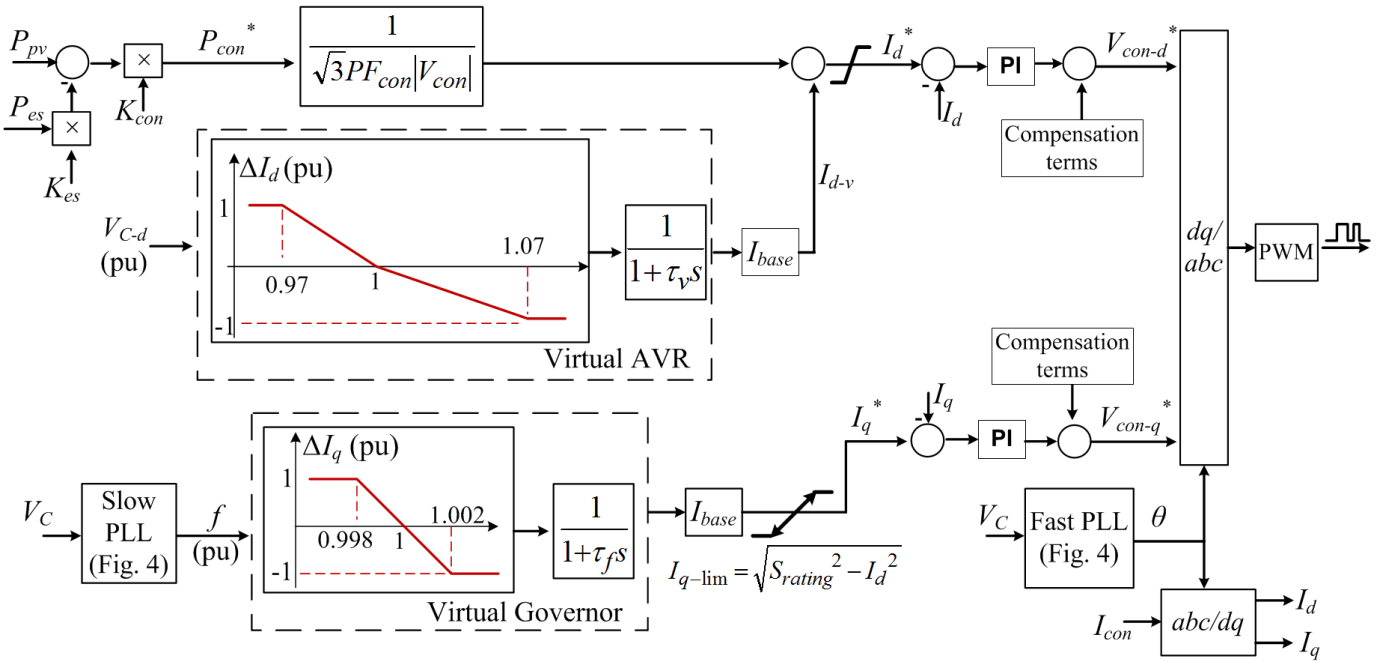

Fig. 3. Proposed DC/AC converter control shown in Fig. 1

1) Controlling the converter power P_{con}:

According to Fig. 1, $P_{pv}=P_{es}+P_{dc}$ (neglecting the converter's loss $P_{dc}=P_{con}$). In order to take into account SoC, the reference converter power is defined as: $P_{con}^{*}=K_{con}(P_{pv}-K_{es}P_{es})$. Therefore, according to Fig. 2.b, whenever:

SoC>90% → $P_{con}^{*}=1(P_{pv}-0\ P_{es})= P_{pv}$

SoC<10% → $P_{con}^{*}=0(P_{pv}-1\ P_{es})= 0 \rightarrow P_{es}=P_{pv}$

10%<Soc<90%→ P_{pv} will be shared between ES and converter according to SoC.

Neglecting $I_{d\text{-}V}$ (in Fig. 3) for now, the reference d-component current I_d^{*} (Fig. 3) will be calculated using, $I_d^{*}=\frac{P_{con}^{*}}{\sqrt{3}\times PF_{con}\times|V_{con}|}$ where, V_{con} and PF_{con} are the converter ac-side voltage and Power Factor.

2) Controlling/supporting frequency:

A synchronous generator, as its name suggests, is synchronized to grid frequency when it is connected to the grid. The system that controls its frequency is called governor. A governor monitors the generator's rotor speed (which is proportional to the grid frequency) and adjusts the input mechanical power from a prime-mover (e.g. a steam turbine) using to a droop characteristic. For example, if speed drops less than the synchronous speed (which means frequency is less than 1 pu) more power is demanded from the prime-mover and vice versa. The same system also controls the frequency in islanded operation of the synchronous generator. Similarly a DG must be synchronised to the grid frequency during grid-connected mode and must be able to control frequency during islanded operation. The common approach in grid-connected mode is to use a PLL to synchronise the DG with the grid, while during islanded mode, droop control is the most common approach to control voltage and frequency of the microgrid. Therefore, since there are two different control schemes, an islanding detection method is required to detect an unplanned islanding event to switch from grid-connected to islanded control. Since grid reconnection is always planned (unlike grid disconnection), it is less problematic. However, there is still some sort of communication from the grid to the DG required to change the control back to grid-connected mode i.e. bringing back the PLL in order to get re-synchronised.

The proposed virtual governor, shown in Fig. 3, is used in both grid-connected and islanded operations; hence, there is no need for an islanding detection method. Moreover, since PLL remains as part of the islanding operation, there is no need for any communication between the grid and DG. The proposed method utilises the combined DG-ES similar to a prime-mover of a synchronous generator. The principal of the operation is explained below:

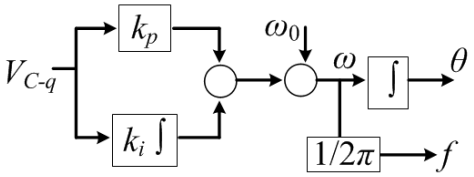

Fig. 4. Schematic diagram of a simple SRF-PLL

The proposed method uses synchronously-reference-frame (SRF)-PLL, which is the most common PLL explained in literature such as [32]. As shown in Fig. 4, the PLL measures frequency through keeping the q-component of filter voltage $V_{C\text{-}q}$=0. As can be seen, the proposed method utilises two PLLs. The reason of using two PLLs will be detailed later on in this section.

Neglecting the filter losses and using Park Transform:

$$P_{con}=\frac{3}{2}\left(V_{C-d}I_d+V_{C-q}I_q\right)$$
$$Q_{con}=\frac{3}{2}\left(V_{C-q}I_d-V_{C-d}I_q\right) \quad (1)$$

Therefore, at steady state when $V_{C\text{-}q}$=0 and $V_{C\text{-}d}\approx$1 pu, active power is proportional to I_d and reactive power is proportional to I_q. It is noted that the responsibility of the PLL in both modes is to make $V_{C\text{-}q}$=0. Thus, it is only needed to control $V_{C\text{-}d}\approx$1 pu in order to support/control voltage. Since the DC-link voltage of the DG is controlled by the ES, after grid disconnection, DG-ES appears as a current source to the local loads. In other words, the local loads impose I_d and I_q at steady state. Since PLL remains as part of the control in islanding operation, P_{con} and Q_{con} remain proportional to I_d and I_q, at steady state (i.e. $V_{C\text{-}q}$=0). For now, assuming there are enough capacity to supply P_L and Q_L, the imposed I_d and I_q, at steady state, will be between +1 pu to – 1pu, which corresponds to an acceptable V and f deviation according to Fig. 3 (voltage -3% and +7%, and frequency ±0.1Hz).

During transient since $V_{C\text{-}q}\neq$0, according to (1), both I_d and I_q are effective in both P and Q (hence, voltage and frequency). However I_d and I_q exhibit different characteristics in respect to frequency variations. Considering Fig. 5, the following equations can be written using KVL and Park Transform:

$$V_{con-d}=V_{C-d}+I_d(R+sL)-L\omega I_q \quad (2)$$
$$V_{con-q}=V_{C-q}+I_q(R+sL)+L\omega I_d \quad (3)$$

where, R and L are filter's resistance and inductance respectively.

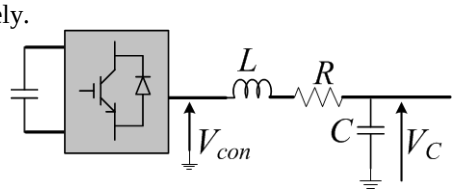

Fig. 5. Schematic diagram of DG's inverter and its filter

According to Fig. 4, one can write:

$$V_{C-q}(k_p+\frac{k_i}{s})+\omega_0=\omega \rightarrow V_{C-q}=\frac{\omega-\omega_0}{k_p+\frac{k_i}{s}} \quad (4)$$

where ω_0 and ω are the reference frequency and measured frequency in rad/s, and k_p and k_i are proportional and integral gains of PLL's PI controller. Since according to (4) $V_{C\text{-}q}$ is a function of frequency, (3) seems more suitable for investigating frequency variations, while (2) seems a better equation for investigating the variation of voltage:

Substituting (4) into (3) and solving it for I_d gives (5) and solving it for I_q gives (6). It is noted that in calculating (5) the assumption is that $\frac{\partial I_q}{\partial\omega}\approx 0$ in comparison with $\frac{\partial I_d}{\partial\omega}$ since I_d is assumed to be the better choice to be actuated by frequency (i.e. more sensitive to frequency variations). Likewise, in calculating (6) the assumption is that $\frac{\partial I_d}{\partial\omega}\approx 0$ compared with $\frac{\partial I_q}{\partial\omega}$ since I_q is assumed more sensitive to frequency variations. Equation (5) shows that $\frac{\partial I_d}{\partial\omega}$ is inversely proportional to ω^2. In other words, as frequency increases, the sensitivity of I_d to change of frequency reduces. On the other hand, according to (6), $\frac{\partial I_q}{\partial\omega}$ is independent of frequency variation. It is noted that the Laplace variables are due to the integration and derivation, not the system's frequency. Therefore, it can be concluded that I_q is a better option for controlling frequency (in comparison to I_d). This may seem contradictory to the well-known fact that (in an inductive system) frequency is proportional to active power. However, it is noted that $|I_{con}|=\sqrt{I_d^{\,2}+I_q^{\,2}}$ and since active power is in fact proportional to $|I_{con}|$, both I_d and I_q can be used to control active power during transient period i.e. when $V_{C\text{-}q}\neq$0. It is also noted that although $\frac{\partial I_q}{\partial\omega}$ is a function of I_d, since inductance L is relatively small and $L\omega I_d$ is added to I_q current control loop as a feedforward compensation term; the effect of I_d can be ignored, hence, $\frac{\partial I_q}{\partial\omega}$ will be mainly effected by the dynamics of PLL (i.e. k_p and k_i).

After the transient (i.e. when $V_{C\text{-}q}$=0), I_q inevitably is imposed by Q_L, which causes a small and within standards deviation of frequency (defined by the droop limits) during islanded operation.

Equation (7) explains the proposed I_q-f droop which is illustrated in Fig. 3:

$$\Delta I_q=K_f\left(f-f_0\right) \quad (7)$$

where f_0 =1 pu (50 Hz in the UK) and K_f is the droop gain. K_f is determined according to the acceptable frequency deviations which may differ in different standard e.g. it is ±0.1 Hz in North EU [33], ±0.2 Hz in Continental EU [33], and ±0.5 Hz in Australia [34].

$$I_d=\frac{V_{con-q}}{L\omega}-\frac{1}{L(k_p+\frac{k_i}{s})}+\frac{\omega_0}{L\omega(k_p+\frac{k_i}{s})}-\frac{I_q(R+sL)}{L\omega}\rightarrow\frac{\partial I_d}{\partial\omega}=\frac{-V_{con-q}}{L\omega^2}-\frac{\omega_0}{L\omega^2(k_p+\frac{k_i}{s})}+\frac{I_q(R+sL)}{L\omega^2} \quad (5)$$

$$I_q=\frac{V_{con-q}}{(R+sL)}-\frac{\omega}{(R+sL)(k_p+\frac{k_i}{s})}+\frac{\omega_0}{(R+sL)(k_p+\frac{k_i}{s})}-\frac{L\omega I_d}{(R+sL)}\rightarrow\frac{\partial I_q}{\partial\omega}=\frac{-1}{(R+sL)(k_p+\frac{k_i}{s})}-\frac{LI_d}{(R+sL)} \quad (6)$$

In Fig. 3 the most restricted standard which is ±0.1 Hz (=±0.002 pu taking 50 Hz as base) is illustrated, however, the proposed method is obviously not limited to this standard. K_f is set such that when frequency deviation is maximum, ΔI_q=±1 pu (K_f=-1/0.002=-500 pu).

Due to a relatively large inertia, the speed of a synchronous generator (hence frequency), which is used in governor, has a relatively slow dynamic. However, the PLL used in DG should have a relatively fast dynamic in order to reduce the transient time and undesirable oscillations at the time of grid reconnection. On the other hand, the measured frequency of the fast PLL does not behave similar to the rotor speed of a synchronous generator. Thus, as illustrated in Fig. 3, it is proposed to use two PLLs: the slow one is used to measure frequency (which is used in virtual governor) while the fast one is used for synchronisation by providing the phase angle θ for the Park Transform. It is noted that: (1) using two PLLs is not the necessary part of the proposed method and the system works with one PLL, but with slightly larger oscillations after grid reconnection. (2) Both PLLs remain part of the control paradigm during islanded operation as well.

Moreover, due to existence of losses (friction and damper bars), any oscillations after a disturbance get damped (assuming stable operation). In order to add similar dynamics and damping characteristics to the proposed control paradigm, a first order low pass filter is augmented to the output of the proposed I_q-f droop (Fig. 3). The following demonstrate that the augmented first order filter exhibits similar characteristics to the dynamics of a synchronous generator:

The rotor dynamics of a synchronous generator is described by swing equation [35]:

$$P_m - P_e = M\ddot{\delta} + D\dot{\delta} \tag{8}$$

where, P_m and P_e are the mechanical input power from prime-mover (in pu) and the generated electrical power (in pu). M is angular momentum which in pu is $M = \frac{H}{\pi f}$, H is inertia constant. D is damping factor and δ is rotor angle. It is known that $\Delta\dot{\delta} = \Delta\omega$ [26], hence equation (8) can be rewritten as:

$$P_m - P_e = M\dot{\omega} + D\omega \rightarrow \Delta P = M\Delta\dot{\omega} + D\Delta\omega \tag{9}$$

In Laplace domain:

$$\Delta P = Ms\Delta\omega + D\Delta\omega \rightarrow \Delta\omega = \frac{\Delta P}{D\left(\frac{M}{D}s + 1\right)} \tag{10}$$

The governor of a synchronous generator utilises the rotor speed deviation from synchronous speed $\Delta\omega$ (which is proportional to the frequency deviation) to actuate the prime-mover. Likewise, the proposed virtual governor, as illustrated in Fig. 3, actuates the prime-mover (i.e. the DG-ES system) by (11):

$$\frac{\Delta I_q}{(\tau_f s + 1)} \tag{11}$$

Therefore, comparing (11) with (10), τ_f can be set proportional to M/D. H is normally between 1-10 pu [35], which makes M=0.0064-0.064 pu (f=50 Hz). Assuming D=0.1 pu, τ_f =0.064-0.64 pu. The output of the virtual governor is then multiplied by base current (I_{base}) and then is limited using a variable ~~hard limit~~ which varies according to $I_{q-\lim} = \sqrt{S_{rating}^2 - I_d^2}$, S_{rating} is the rated apparent power of the DG's converter. It is noted that at steady state I_q is proportional to reactive power. If converter's capacity is not sufficient to supply load reactive power Q_L, AG will supply the difference using the scheme explained in section C.

3) Controlling/supporting voltage:

In a synchronous generator an automatic voltage regulator (AVR) is used to control the terminal voltage of the generator (V_t) through varying its excitation current (I_f). Fig. 3 proposes a virtual AVR which augments the d-component current from the P_{con} control scheme by $I_{d\text{-}v}$ to form I_d^*. As discussed above, since at steady state $V_{C\text{-}q}$=0, P and Q are proportional to I_d and I_q respectively. However, during transient since $V_{C\text{-}q}\neq$0, both I_d and I_q can be used to control P and Q. The followings demonstrate that I_d (compared to I_q) is a better option for controlling voltage:

Equation (2) can be rewritten as:

$$\Delta V_d = I_d(R + sL) - L\omega I_q \tag{12}$$

where, ΔV_d is the d-component of the voltage drop across the filter's impedance. Solving (12) for I_q gives:

$$I_q = \frac{I_d(R + sL)}{L\omega} - \frac{\Delta V_d}{L\omega} \rightarrow \frac{\partial I_q}{\partial \Delta V_d} = \frac{-1}{L\omega} \tag{13}$$

Solving (12) for I_d gives:

$$I_d = \frac{I_q L\omega}{R + sL} + \frac{\Delta V_d}{R + sL} \rightarrow \frac{\partial I_d}{\partial \Delta V_d} = \frac{1}{R + sL} \tag{14}$$

It is noted that in calculating (13) the assumption is that $\frac{\partial I_q}{\partial \Delta V_d} \approx 0$ compared with $\frac{\partial I_d}{\partial \Delta V_d}$ since I_q is assumed to be more sensitive to voltage variations (i.e. the better choice). Similarly, in calculating (14) the assumption is that $\frac{\partial I_d}{\partial \Delta V_d} \approx 0$ compared with $\frac{\partial I_q}{\partial \Delta V_d}$ as I_d is chosen to be actuated by voltage variations. Equation (13) demonstrates that $\frac{\partial I_q}{\partial \Delta V_d}$ is inversely proportional to ω. Therefore, as frequency increases, the sensitivity of I_q to voltage variations reduces. However according to (14), $\frac{\partial I_d}{\partial \Delta V_d}$ only depends on filter's impedance.

Hence, I_d is a better option for controlling voltage. After the transient (i.e. when $V_{C\text{-}q}$=0), I_d inevitably is imposed by P_L, which causes a small and within standards deviation of voltage (defined by the droop limits) during islanded operation.
Equation (15) explains the proposed I_d-V droop illustrated in Fig. 3:

$$\Delta I_d = K_v(V - V_0) \tag{15}$$

where, V and V_0 are the measured and reference voltages (V_0=1 pu), and K_v is the voltage droop gain. K_v is determined according to the acceptable voltage deviations defined by standards: 0.94 pu<V<1.1 pu [10], [34]. Assuming 3% voltage drop on transformers/transmission line, voltage variation used in Fig. 3 will be: 0.97 pu<V<1.07 pu. K_v is defined such that when V=0.97 pu, ΔI_d=1 pu; and when V=1.07 pu, ΔI_d=-1 pu: K_v= -33.33 pu for V<1 pu, and K_v=-14.28 pu for V>1 pu. Similar to the virtual governor, the output of the I_d-V droop is passed through a first order low-pass filter in order to add dynamics and damping characteristic to the system.

Fig. 6 shows a simplified diagram of a static AVR system [36] (used in synchronous generators) where, R_e and L_e are the resistance and the inductance of the synchronous generator's excitation winding; V_0 and V_t are the reference and terminal voltage of the generator; and I_f is the excitation current.

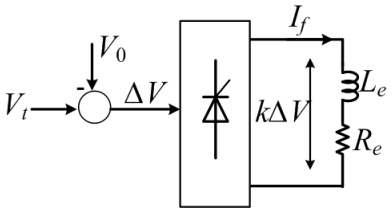

Fig. 6. Simplified Schematic of a static AVR system

As the voltage error ΔV varies, I_f varies accordingly (using the thyristor bridge) in order to control the generator's excitation. Thus, it can be concluded that the voltage across the excitation winding is proportional (assuming a linear magnetisation) to ΔV. Thus:

$$K\Delta V = I_f(R_e + sL_e) \rightarrow I_f = \frac{K\Delta V}{R_e\left(\frac{L_e}{R_e}s + 1\right)} \tag{16}$$

According to (15), the output of the proposed virtual AVR, shown in Fig. 3:

$$I_{d-v} = \frac{K_v(V - V_0)}{1 + \tau_v s} \tag{17}$$

Comparing (17) with (16) demonstrates that τ_v is proportional to L_e/R_e. An AVR system is much faster than a governor, hence, τ_v =0.02-0.1 pu seems appropriate.

C. Auxiliary Generator Control

The AG is a fossil-fuelled generator (e.g. a microturbine). Hence, the idea is to minimise its usage through controlling it as a back-up for active and reactive power compensation. Although not considered in this paper, it is possible to use a demand side management scheme prior to turning on the AG in order to reduce the AG's required rating to a value enough to supply only the critical loads.

Active power control of AG is illustrated in Fig. 1 and Fig. 2.b. In this paper the AG does not make any contribution in load active power P_L during grid-connected mode (it is obviously possible to do so, if required). Hence, the load is shared between the DG and the grid. The ratio of sharing depends on generated solar energy and how much energy the owner of the DG wants to store (here assumed 90% of ES capacity). In islanded mode the load is mainly supplied by the DG-ES. Since the DC-link voltage is controlled by ES's DC/DC converter, SoC is an indicator of shortage (or excess) of energy. For SoC < a threshold (e.g. 30%) a demand signal will be sent to the AG which increases as SoC drops such that when (e.g.) SoC=5%, P_{ag}^*=1 pu. Obviously, it is also possible to use load shedding schemes prior to bringing in the AG in order to supply only the critical loads by the AG.

In this paper the DG's converter does not make any contribution in load reactive power Q_L during grid-connection mode. However if required, it is possible to augment the reference I_q^* form the virtual governor with another reference to supply part of Q_L during grid-connected operation.

During islanded operation, Q_L will be supplied by the converter. Since both P_L and Q_L are (initially) supplied by the DG-ES, measures must be taken into account to make sure that the DG's converter rating S_{rating} is not violated. In order to achieve this, it is proposed in Fig. 1 to utilise the AG when Q_L is high: As shown in Fig. 1, Q_{con} is limited using a variable hard limit which varies according to $Q_{\text{limit}} = \sqrt{S_{sm}^2 - P_{con}^2}$ (since P_{con} changes, a variable hard limit is needed), where S_{sm} = S_{rating} -0.03 pu (0.03 pu is a proposed safety margin). Then, the limited Q_{con} is subtracted from (the unlimited) Q_{con} to constitute the error reactive power Q_e (hence, as long as Q_{con}<Q_{limit} $\rightarrow Q_e$=0). Q_e is controlled to zero using a PI controller actuating the reference AG's reactive power Q_{ag}*. The integrator of the PI controller will be rest when Q_{con}<(Q_{limit}-0.03 pu), 0.03 pu is a suggestion to make sure that Q_{con}<<Q_{limit}, hence, avoiding possible oscillation. If the integrator is not reset, Q_L will be shared by the converter and the AG even when Q_L<Q_{limit}. It is noted that a local communication between the DG and the AG is required to communicate P_{ag}^* and Q_{ag}^*.

III. Simulation Results

The model shown in Fig. 1 was simulated in PSCAD/EMTDC environment. The PV converter's S_{rating}=1.1 pu (based on PV array rating). Considering 3% safety margin S_{mt}=1.07 pu. The rest of the parameters are given in Table I.

Two scenarios are simulated:

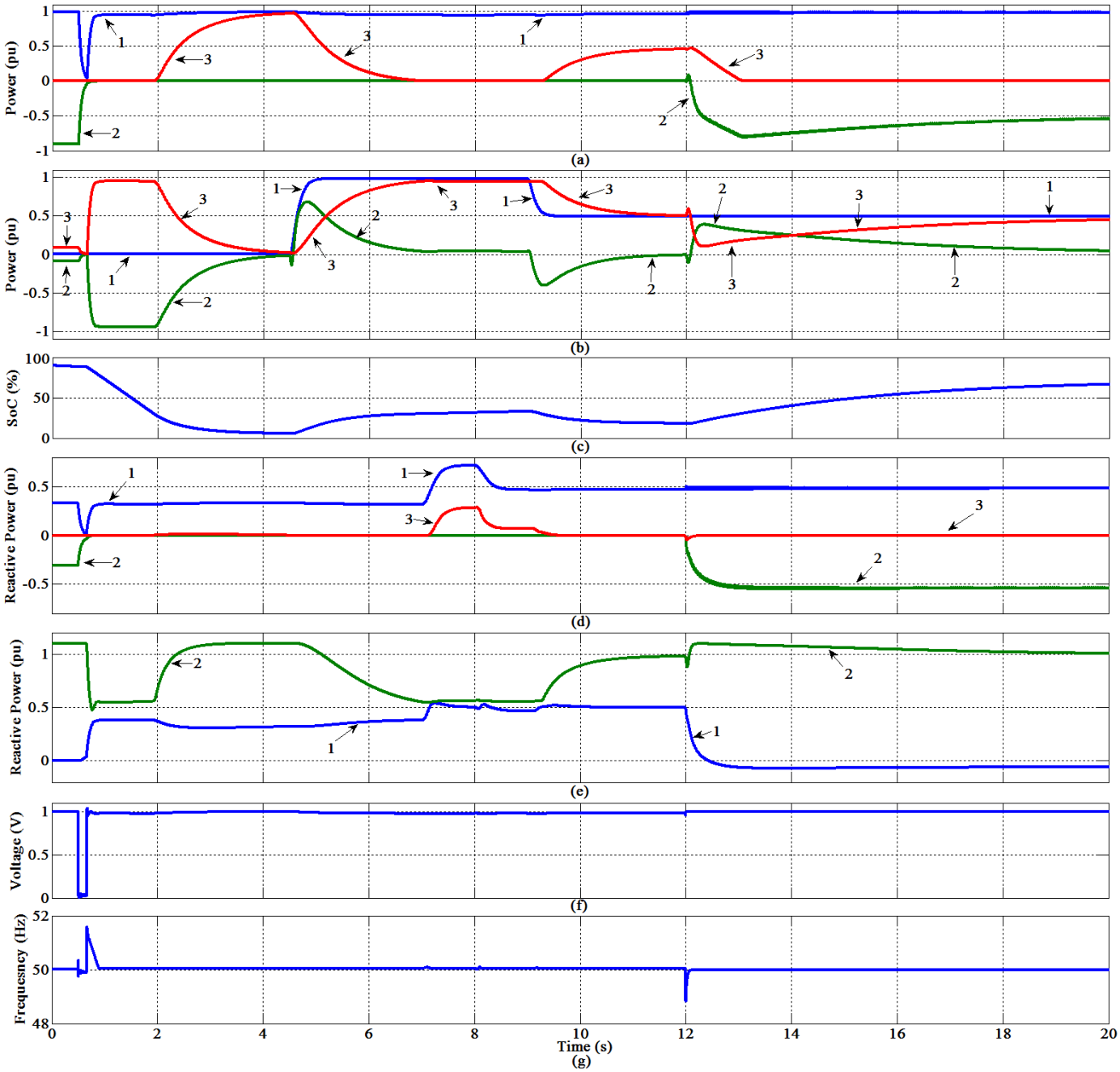

Fig. 7. Simulation results for $P_{pv} \leq P_L$ during islanding operation: (a) active power, pu 1-P_L, 2-P_g, 3-P_{ag} (b) active power, pu 1-P_{pv}, 2-P_{es}, 3-P_{con} (c) battery's SoC, % (d) reactive power, pu 1-Q_L, 2-Q_g, 3-Q_{ag} (e) reactive power, pu 1-Q_{con}, 2-Q_{limit} (f) V_{pcc}, pu (g) frequency, Hz

A. During Islanding $P_{pv} \leq P_L$

The simulation results are shown in Fig. 7. The simulation events are as follows: 0-0.5 s, P_L=1 pu with PF=0.95 lagging. Since P_{pv}=0, grid supplies load P_L and Q_L. SoC is assumed 90%. It is noted that since due to voltage drops on transformers and transmission line impedances, V_C<1 pu, the proposed virtual AVR uses the energy stored in ES to restore the voltage. In practical systems this is normally done using transformer's tap changer, which was intentionally removed to demonstrate the ability of the proposed scheme to support local voltage in case of weak grids.

Table I. System's parameters

Variable	Value
Filter impedance Z_f	R=1 mΩ L=0.1 mH
Transformers' leakage reactance	10%
Transmission line impedance Z_t	R=0.16 Ω L=0.6 mH
Current loops PI controllers	K_p= 0.157 K_i=1.57 (using pole placement)
τ_f , τ_v and τ_d	0.3 pu , 0.05 pu and 0.05 pu
AG's reactive power PI controller	K_p=2 K_i=17
PLLs' PI controller (fast/slow)	K_p=15/5 K_i=0.2/10

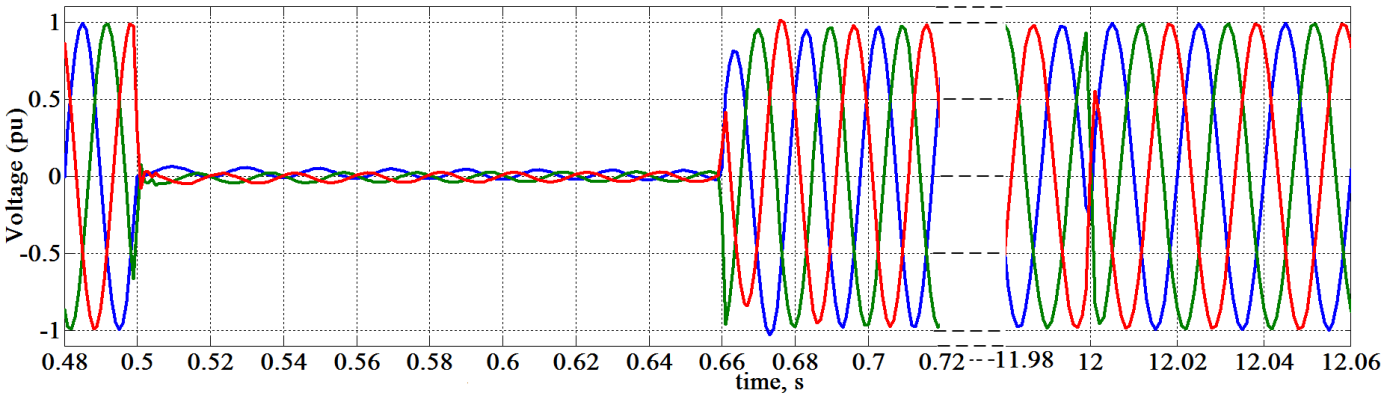

Fig. 8. The three-phase voltage waveform of V_{pcc} (pu) for the simulation events shown in Fig. 7.

At t=0.5 s a 3-phase fault occurs at the grid-side and after 0.16 s (standard delay for relays operation), the circuit breaker (CB) opens:

1) Islanded operation (0.5-12 s):

Fig. 7.f&g show that voltage of point of common coupling V_{pcc} and f are very well-controlled (note that just before fault P_L=P_g=1pu i.e. the worst case scenario in terms of power imbalance). Fig. 7.g depicts the measured frequency by the slow PLL as it is used in the virtual governor. The reduction in P_L is due to a slight reduction in voltage (V_{pcc}= 0.97 pu which is within the acceptable limits). P_L is supplied by ES through P_{con} (Fig. 7.b) and Q_L is supplied by PV converter (Q_{con}, Fig. 7.e). When SoC<30% (happens at t≈2 s), P_{ag} increases to supply P_L (Fig. 7.a). Using the proposed method, when SoC=5%, P_{ag}= P_L=1pu. At t=4.5 s, P_{pv} increases to 1pu. Since SoC<10%, first ES power P_{es} (Fig. 7.b) increases, then as SoC increases, P_{con} increases which causes P_{es} and P_{ag} to reduce (note that due to V_{pcc}=0.97pu, P_L (=P_{con}) is slightly less than 1pu, hence, for P_{pv}=1pu, some power will be still available for ES). It is noted that Q_{limit} (Fig. 7.e) drops as P_{con} increases (i.e. less capacity for Q support is available). As a result, when at t=7 s, PF drops to 0.8 lagging, Q_L>Q_{limit} (Fig. 7.d &e). The proposed scheme makes sure that Q_{con} does not violate its limit (Fig. 7.e) through supplying the difference by the AG Q_{ag} (Fig. 7.d). At t=8 s, PF increases to 0.9 lagging, which causes Q_L, hence, Q_{ag} to reduce. However, since Q_{con} is not less than (Q_{limit}-0.03pu), the PI controller is not reset, leading to Q_{ag}≠0. At t=9 s, P_{pv} drops to 0.5 pu, SoC reduces to supply the shortage. Again when SoC<30%, P_{ag} increases to feed load. When P_{ag} supplies the load, P_{con} reduces which in turn causes to Q_{limit} to increase i.e. more capacity from the converter to supply reactive power. As a result, Q_{con}<(Q_{limit}-0.03pu), which reset the PI controller, hence, Q_{ag}=0.

2) Grid Reconnection:

At t=12 s, CB is closed and voltage and frequency are restored. After a short transient (about 0.2 s), Q_{con}=Q_{ag}=0, Q_g=Q_L=0.5 pu (PF=0.9 lag). As discussed, it is possible to supply part of Q_L using the converter if required. It can be seen than after reconnection, since SoC is less than 90%, first P_{es} increases. However, as SoC increases toward 90%, P_{es} reduces and P_{con} increases. It is emphasised again that the 90% threshold can be set by the owner/operator of the DG and theoretically can be any value. Fig. 8 illustrates the 3-phase waveform of V_{pcc} (for the simulation events of Fig. 7), which is zoomed in at the time of fault (0.5 s) and grid reconnection (12 s). This demonstrates that both voltage and frequency are controlled within standards during both operational modes.

B. During Islanding P_L≤P_{pv}

In islanding operation it is possible that P_{pv}>P_L for longer than the capacity of ES. In such cases different "dumping" mechanisms are introduced in literature, most of them include a dumping resistance. This paper proposes to reduce the generation through altering V_{dc}^*, which is produced by MPPT algorithm, as illustrated in Fig. 2. Since V_{dc}^* is a unique voltage (for each solar irradiance) at which P_{pv} is maximum, adding a gain (K_d) to it will reduce the generated power. It should be emphasised that the proposed dumping algorithm is not the necessary part of the proposed voltage and frequency control and any other dumping methods such as those introduced in [2], [3], and [37] can be used as well.

The simulation results are shown in Fig. 9: initially P_{pv}=P_L=0.5 pu. Since SoC<90% (Fig. 9.c), P_{pv} is shared between P_{con} and P_{es} (Fig. 9.b). However, since SoC is close to 90%, P_{con}≈P_{pv}>>P_{es} (Fig. 9.b). The difference between P_L and P_{con} is supplied by P_g (Fig. 9.a), until t=0.5 s, when a three phase fault occurs (Fig. 1) and after 0.16 s, the CB is opened. Hence, P_{con}=P_{pv}=P_L=0.5 pu. At t=1.5 s, P_{pv} increases to 0.75 pu. Since P_{pv}>P_L, the difference is stored in ES causing SoC to increase. Using the proposed voltage control in Fig. 3, $I_{d\text{-}v}$ is reduced to keep V_{pcc} less than 1.1 pu as shown in Fig. 9.e. As SoC>95%, (happens at t≈2.8 s) according to the proposed method shown in Fig. 2, K_d, (with the rate of 50 and τ_d=0.05) is added to V_{dc}* hence, P_{pv} reduces =P_{con}=P_L (Fig. 9.b). As a result SoC remains constant at almost 97%. At t=4.5 s, P_L increases to 1 pu, hence SoC reduces to compensate for the shortage which causes K_d=0, hence, P_{pv} returns back to its maximum value (0.75 pu). At t=6 s, grid is re-connected, hence, V and f are restored. Since SoC=85% (very close to 90%), P_{con}≈P_{pv}=0.75 pu (P_{es}≈0), and P_g supplies the difference between P_L and P_{con}. Fig. 9.d shows that $V_{C\text{-}q}$≈0 at steady state even during islanded operation (0.5-5.5 s).

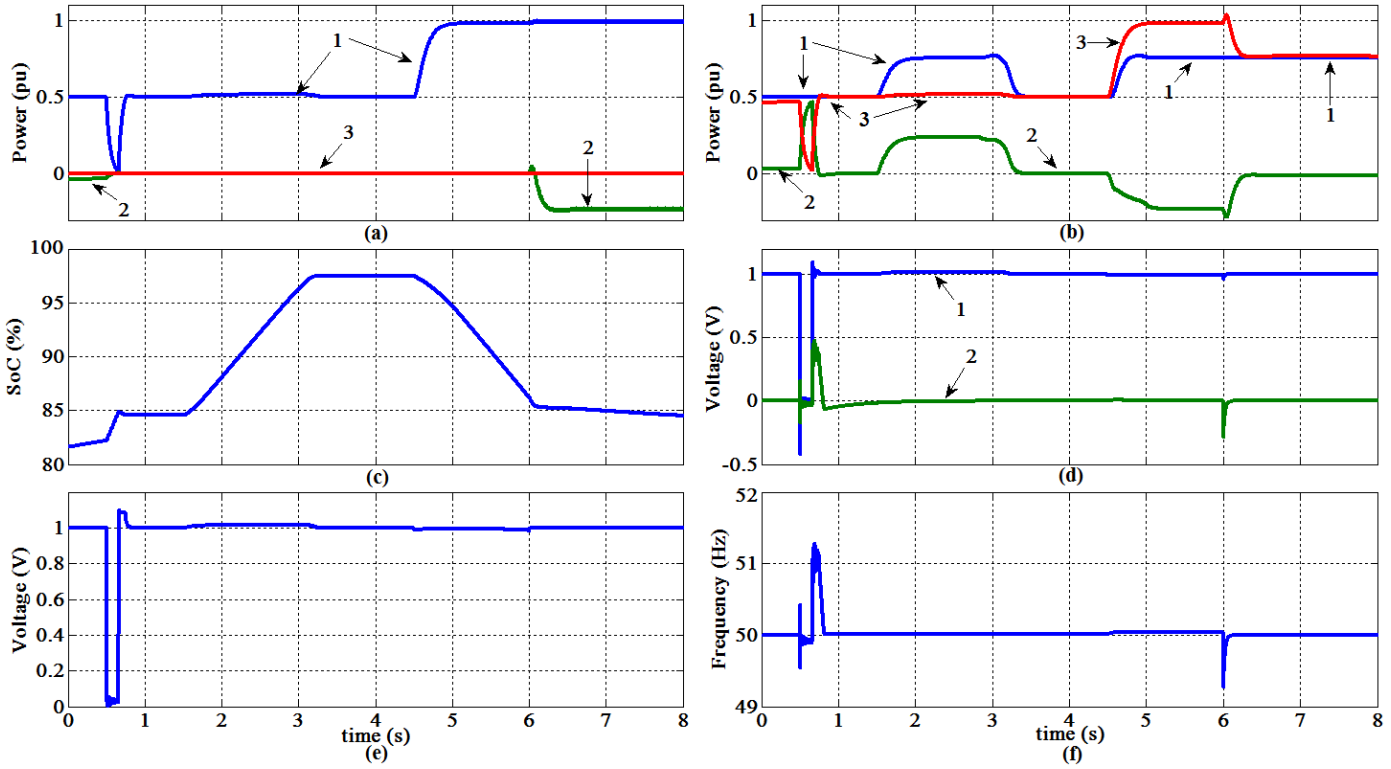

Fig. 9. ES over-charge protection: (a) power, pu 1-P_L, 2-P_g, 3-P_{ag} (b) power, pu 1-P_{pv}, 2-P_{es}, 3-P_{con} (c) battery's SoC%, (d) voltage, pu 1-$V_{C\text{-}d}$, 2-$V_{C\text{-}q}$ (e) V_{pcc}, pu (f) frequency, Hz

IV. Conclusion

A universal control paradigm for microgrids has been introduced that seamlessly rides-through a fault on the grid side, control voltage and frequency locally, and seamlessly get synchronised to the grid upon grid reconnection. An energy storage control is introduced that controls the DC-link voltage of a distributed resource to track the maximum power while its energy level (here SoC) is managed through a comprehensive active power management scheme. The active power management scheme uses the energy level of the energy storage to determine how much energy is being stored or is being passed to the grid/load. The desired stored energy level can be set by the owner/operator of the distributed generator/grid. It is also possible to introduce a scheme to sell the stored energy, if required. The control scheme utilises the combined distributed generator-energy storage units similar to a prime-mover of a synchronous generator. If the energy level becomes less than a threshold, an auxiliary generator supplies the shortage. If the energy level becomes more than a threshold, the proposed scheme reduces the generated power, rather than dumping it using a resistance. A comprehensive reactive power management scheme is also introduced that utilises all the available capacity of the distributed generator's converter while making sure that its rating is not violated through supplying/absorbing the remaining load reactive power by the auxiliary generator.

Actuating I_d by voltage error may seem as a disadvantage, for inductive microgrids, where I_q is traditionally used for voltage control. However, the added advantage of a simple and effective fault ride-through capability surely outweighs the drawback. Moreover, other methods such as transformers' tap changer can be used to minimise the usage of DG-ES to control voltage.

V. References

[1] D. E. Olivares, A. Mehrizi-Sani, A. H. Etemadi, C. A. Cañizares, R. Iravani, M. Kazerani, A. H. Hajimiragha, O. Gomis-Bellmunt, M. Saeedifard, R. Palma-Behnke, G. A. Jiménez-Estévez, and N. D. Hatziargyriou, "Trends in Microgrid Control," *IEEE Trans. on Smart Grid*, vol. 5, no. 4, pp. 1905 – 1919, July 2014.

[2] M. Fazeli, G. Asher, C. Klumpner, L. Yao, and M. Bazargan, "Novel Integration of Wind Generator-Energy Storage Systems Within Microgrids," *IEEE Trans. on Smart Grid*, vol. 3, no. 2, pp. 728 – 737, June 2012.

[3] M. Fazeli, G. Asher, C. Klumpner, and L. Yao, "Novel Integration of DFIG-Based Wind Generators Within Microgrids," *IEEE Trans. on Energy Convers.*, vol. 26, no. 3, pp. 840 – 850, Sep. 2011.

[4] F. Katiraei, M. R. Iravani, and P. W. Lehn, "Micro-grid autonomous operation during and subsequent to islanding process," *IEEE Traans. on Power Del.*, vol. 20, no. 1, pp. 248 – 257, Jan. 2005.

[5] H. Laaksonen, " Advanced Islanding Detection Functionality for Future Electricity Distribution Networks," *IEEE Trans. on Power Del.*, vol. 28, no. 3, pp. 2056 – 2064, Oct. 2013.

[6] H. H. Zeineldin, "A Q – f Droop Curve for Facilitating Islanding Detection of Inverter-Based Distributed Generation," *IEEE Trans. on Power Electron.*, vol. 24, no. 3, pp. March 2009.

[7] J. Merino, P. Mendoza-Araya, G. Venkataramanan, and M. Baysal, "Islanding Detection in Microgrids Using Harmonic Signatures," *IEEE Trans. on Power Del.*, vol. 30, no. 5, pp. 2102 – 2109, Oct. 2015.

[8] H. Karimi, H. Nikkhajoei, and R. Iravani, "Control of an Electronically-Coupled Distributed Resource Unit Subsequent to an Islanding Event," *IEEE Trans. on Power Del.*, vol. 23, no. 1, pp. 493 – 501, Jan. 2008.

[9] A. M. Egwebe, M. Fazeli, P. Igic, and P. M. Holland, "Implementation and stability study of Dynamic Droop in islanded MicroGrids," *IEEE Trans. on Energy Convers.*, vol. pp, no. 99, pp. 821 – 832, Sep. 2016.

[10] M. Fazeli, J. B. Ekanayake, P. M. Holland, and P. Igic, "Exploiting PV Inverters to Support Local Voltage—A Small-Signal Model," *IEEE Trans. on Energy Convers.*, vol. 29, no. 2, pp. 453 – 462, June 2014.

[11] IEEE, "Standard for Interconnecting Distributed Resources with Electric Power Systems, IEEE Std. 1547," ed, 2003.

[12] S. T. Sushil and V. Agarwal, "Controller Area Network Assisted Grid Synchronization of a Microgrid With Renewable Energy Sources and Storage," *IEEE Trans. on Smart Grid*, vol. 7, no. 3, pp. 1442 – 1452, May 2016.

[13] P. Rodríguez, A. Luna, R. S. Muñoz-Aguilar, L. Etxeberria-Otadui, R. Teodorescu, and F. Blaabjerg, "A Stationary Reference Frame Grid Synchronization System for Three-Phase Grid-Connected Power Converters Under Adverse Grid Conditions," *IEEE Trans. on Power Electron.*, vol. 27, no, 1, pp. 99 – 112, Jan. 2012.

[14] Y. F. Wang and Y. W. Li, "Grid Synchronization PLL Based on Cascaded Delayed Signal Cancellation," *IEEE Trans. on Power Electron.*, vol. 26, no, 7, pp. 1987 – 1997, July 2011.

[15] F. De Mango, M. Liserre, A. Aquila, and A. Pigazo, "Overview of anti-islanding algorithms for PV systems. Part I: Passive methods," in *12th Int. Power Electron. Motion Control Conf.*, Sep. 2006, pp. 1878-1883.

[16] A. Aljankawey, W. Morsi, L. Chang, and C. Diduch, "Passive methodbased islanding detection of renewable-based distributed generation: The issues," in *IEEE Elect. Power Energy Conf*, Aug. 2010, pp. 1-8.

[17] B. Singam and L. Hui, "Assessing SMS and PJD schemes of anti-islanding with varying quality factor," in *IEEE Int. Power Energy Conf.*, Nov. 2006, pp. 196-201.

[18] M. Bakhshi, R. Noroozian, and G. Gharehpetian, "Passive anti-islanding scheme based on reactive power in the smart grids," presented at the 2nd Iranian Conf. Smart Grids, May 2012.

[19] A. Samui and S. Samantaray, "Assessment of ROCPAD relay for islanding detection in distributed generation," *IEEE Trans. Smart Grid,*, vol. 2, no. 2, pp. 391-398, pp. 391 – 398, June 2011.

[20] H. Karegar and A. Shataee, "Islanding detection of wind farms by THD," in *3 rd Int. Conf. Elect. Utility Dereg. Restruct. Power Technol.*, Apr. 2008, pp. 2793-2797.

[21] G. Hernandez-Gonzalez and R. Iravani, "Current injection for active islanding detection of electronically-interfaced distributed resources," *IEEE Trans. on Power Del.*, vol. 21, no. 3, pp. 1698-1705, Jul. 2006.

[22] F. Liu, Y. Kang, Y. Zhang, S. Duan, and X. Lin, "Improved SMS islanding detection method for grid-connected converters," *IET Rene. Power Gen.*, vol. 4, no. 1, pp. 36-42, Jan. 2010.

[23] D. Velasco, C. Trujillo, G. Garcera, and E. Figueres, "An active anti-islanding method based on phase-PLL perturbation," *IEEE Trans. on Power Electron.*, vol. 26, no. 4, pp. 1056-1066, Apr. 2011.

[24] M. Ciobotaru, V. Agelidis, R. Teodorescu, and F. Blaabjerg, "Accurate and less-disturbing active antiislanding method based on PLL for gridconnected converters," *IEEE Transaction on Power Electronics*, vol. 25, no. 6, pp. 1576-1584, Jun. 2010.

[25] H. Karimi, A. Yazdani, and M. R. Iravani, "Negative-sequence current injection for fast islanding detection of a distributed resource unit," *IEEE Trans. on Power Electron.*, vol. 23, no. 1, pp. 298-307, Jan. 2008.

[26] S. M. Ashabani and Y. A.-r. I. Mohamed, "New Family of Microgrid Control and Management Strategies in Smart Distribution Grids-Analysis, Comparison and Testing," *IEEE Trans. on Power Syst.*, vol. 29, No. 5, pp. 2257 – 2269, Sep. 2014.

[27] M. Guan, W. Pan, J. Zhang, Q. Hao, J. Cheng, and X. Zheng, "Synchronous Generator Emulation Control Strategy for Voltage Source Converter (VSC) Stations," *IEEE Trans. on Power Syst.*, vol. 30, no. 6, pp. 3093 – 3101, Nov. 2015.

[28] H. Alatrash, A. Mensah, E. Mark, G. Haddad, and J. Enslin, "Generator Emulation Controls for Photovoltaic Inverters," *IEEE Trans. on Smart Grid*, vol. 3, no. 2, pp. 996 – 1011, June 2012.

[29] J. Liu, Y. Miura, and T. Ise, "Comparison of Dynamic Characteristics Between Virtual Synchronous Generator and Droop Control in Inverter-Based Distributed Generators," *IEEE Trans. on Power Electron.*, vol. 31, no. 5, pp. 3600 – 3611, May 2016.

[30] M. Karimi-Ghartemani, "Universal Integrated Synchronization and Control for Single-Phase DC/AC Converters," *IEEE Trans. on Power Electron.*, vol. 30, no. 3, pp. 1544 – 1557, March 2015.

[31] M. Fazeli, P. Igic, P. M. Holland, R. P. Lewis, and Z. Zhou, "Novel Maximum Power Point Tracking with classical cascaded voltage and current loops for photovoltaic systems," presented at the IET Conference on Renewable Power Generation RPG Edinburgh, UK, 2011.

[32] S. Golestan and J. M. Guerrero, "Conventional Synchronous Reference Frame Phase-Locked Loop is an Adaptive Complex Filter," *IEEE Trans. on Indus. Electron.*, vol. 62, no. 3, pp. 1679 – 1682, March 2015.

[33] J. M. Guerrero, J. C. Vasquez, J. Matas, L. G. de Vicuna, and M. Castilla, "Hierarchical control of droop-controlled AC and DC microgrids—a general approach toward standardization," *IEEE Trans. on Indus. Electron.*, vol. 58, no. 1, pp. 158 – 172, Jan. 2011.

[34] T. Morstyn, B. Hredzak, and V. G. Agelidis, "Distributed Cooperative Control of Microgrid Storage," *IEEE Trans. on Power Syst.*, vol. 30, no. 5, pp. 2780 – 2789, Sep. 2015.

[35] J. D. Glover, M. S. Sarma, and T. J. Overbye, "Transient Stability" in *Power System Analysis & Design*, 5 ed. USA: CENGAGE Learning, 2012, pp. 591.

[36] N. Jenkins, J. B. Ekanayake, and G. Strbac, "AC machines" in *Distributed Generation*: IET, 2010, pp. 212.

[37] T. Lukasievicz, R. V. de Oliveira, and G. G. Dranka, "Control of an islanded wind-diesel microgrid with high penetration level of wind generation," in *2015 IEEE Power & Energy Society General Meeting*, 2015, pp. 1 - 5.